Available online at www.sciencedirect.com

ScienceDirect

Polar Science 4 (2011) 497–514

NiPR National Institute of Polar Research

http://ees.elsevier.com/polar/

Petrology and geochemistry of Yamato 984028: a cumulate lherzolitic shergottite with affinities to Y 000027, Y 000047, and Y 000097

Amy J.V. Riches [a,*], Yang Liu [a], James M.D. Day [b], Igor S. Puchtel [b], Douglas Rumble III[c], Harry Y. McSween Jr.[a], Richard J. Walker [b], Lawrence A. Taylor [a]

[a] *Planetary Geosciences Institute, Department of Earth & Planetary Sciences, University of Tennessee, Knoxville, TN 37996, USA*
[b] *Department of Geology, University of Maryland, College Park, MD 20742, USA*
[c] *Geophysical Laboratory, Carnegie Institution of Washington, Washington DC 20015, USA*

Received 30 July 2009; revised 20 March 2010; accepted 26 April 2010
Available online 13 May 2010

Abstract

We report the petrography, mineral and whole-rock chemistry (major-, trace-, and highly-siderophile element abundances, and osmium and oxygen isotope compositions) of a newly recognized lherzolitic shergottite, Yamato (Y) 984028. Oxygen isotopes ($\Delta^{17}O = 0.218‰$) confirm a martian origin for this meteorite. Three texturally distinctive internal zones and a partially devitrified fusion crust occur in the polished section of Y 984028 studied here. The zones include: 1) a poikilitic region with pyroxene enclosing olivine and chromite (Zone A); 2) a non-poikilitic zone with cumulate olivine, interstitial pyroxene, maskelynite and Ti-rich chromite (Zone B) and; 3) a monomict breccia (Zone C). The pyroxene oikocryst in Zone A is chemically zoned from $Wo_{3-7}En_{76-71}$ in the core region to $Wo_{33-36}En_{52-49}$ at the rim, and encloses more Mg-rich olivine (Fo_{74-70}) in the core, as compared with olivines (Fo_{69-68}) located at the oikocryst rim. Constraints from Fe–Mg partitioning between crystals and melt indicate that constituent minerals are not in equilibrium with the corresponding bulk-rock composition, implying that Y 984028 represents a cumulate. The whole-rock major- and trace-element compositions, and initial $^{187}Os/^{188}Os$ value (0.1281 ± 0.0002) of Y 984028 are similar to other lherzolitic shergottites and this sample is probably launch-paired with Y 793602, Y 000027, Y 000047, and Y 000097. The Os isotopic composition and highly-siderophile element (HSE) abundances of Y 984028 and other lherzolitic shergottites are consistent with derivation from a martian mantle source that evolved with chondritic Re/Os.

Keywords: Lherzolitic; Shergottite; Petrology; Geochemistry; Osmium; Mars

1. Introduction

Shergottites are achondrites that are widely regarded as martian magmatic rocks (e.g., Bogard and Johnson, 1983; McSween, 1994; McSween and Treiman, 1998; Treiman et al., 2000). These meteorites are among a limited number (~55, after pairing; Meyer, 2009) recognized as direct samples from Mars, which present an opportunity to constrain the nature and timing of igneous processes that operated on the red-planet. Shergottites are traditionally divided into

* Corresponding author. Tel.: +1 865 974 6024.
E-mail address: ariches@utk.edu (A.J.V. Riches).

1873-9652/$ - see front matter © 2010 Elsevier B.V. and NIPR. All rights reserved.
doi:10.1016/j.polar.2010.04.009

three groups based on their textures and mineralogy (e.g., McSween, 2002): 1) fine-grained basaltic shergottites, containing abundant clinopyroxene, pigeonite, and maskelynite; 2) olivine- (± pyroxene) phyric shergottites, with olivine and orthopyroxene megacrysts in a fine-grained basaltic matrix; and 3) lherzolitic shergottites, containing olivine poikilitically enclosed by pyroxenes and a non-poikilitic lithology, with olivine and interstitial pyroxene, maskelynite, and minor phases. Shergottites can also be classified into three different chemical groups based on their incompatible trace-element inventories: 1) enriched shergottites, including most basaltic shergottites and a few olivine-phyric shergottites (Northwest Africa [NWA] 1068, Larkman Nunatak [LAR] 06319, Roberts Massif [RBT] 04262); 2) highly-depleted shergottites, including most olivine-phyric shergottites and one basaltic shergottite (Queen Alexandra Range [QUE] 94201); and 3) intermediate shergottites, including all lherzolitic shergottites and Elephant Moraine (EETA) 79001 (e.g., Lodders, 1998; Goodrich, 2002; McSween, 2002; Basu Sarbadhikari et al., 2009).

A petrogenetic interpretation of the relationships among all three chemical groups of shergottites is the subject of considerable debate. Enriched shergottites may be related to highly-depleted and intermediate shergottites by the assimilation of relatively evolved and oxidized martian crust (Jones, 1989; Wadhwa, 2001; Herd et al., 2002). Alternatively, trace-element and isotopic diversity in depleted, enriched, and intermediate shergottites may reflect chemically diverse mantle sources (Herd et al., 2002; Borg and Draper, 2003; Symes et al., 2008; Basu Sarbadhikari et al., 2009). Complimentary to constraints provided by lithophile elements and their isotope systems, the Re–Os isotope system combined with highly-siderophile element abundances (HSE; Os, Ir, Ru, Pt, Pd, and Re) may offer important insight for discriminating between these petrogenetic models. In addition, the abundance and isotopic systematics of these elements in relatively primitive lherzolitic shergottites provide unique information that has been used to constrain martian mantle evolution (e.g., Warren et al., 1999; Brandon et al., 2000; Walker, 2009).

As part of the mini-consortium formed by the National Institute of Polar Research, (NIPR; Japan) to study Yamato (Y) 984028, we present detailed petrographic, mineralogical, and geochemical characteristics of this meteorite with which to constrain its petrogenesis. Y 984028 (12.3 g) was discovered partially covered with a fusion crust in an ice field north of the JARE IV Nunatak in Antarctica. The sample was identified as a lherzolitic shergottite (NIPR Meteorite Newsletter 17, 2008), complementing 12 other lherzolitic shergottites identified to date. The collection site of Y 984028 is proximal to the area where the lherzolitic shergottites Y 000027, Y 000047, and Y 000097 were found (Misawa et al., 2009). Lherzolitic shergottites are thought to be derived from relatively primitive melts that sample the martian mantle (McSween, 2003), providing information of the igneous processes responsible for creating portions of Mars' mafic crust (which differs from spectroscopic observations of the martian surface, e.g., McSween et al., 2009), as well as indirect information of martian mantle composition.

2. Methodology

2.1. Mineral analysis

A polished section (#51-3; ~0.2 cm^2) of Y 984028 was provided by NIPR. The major-element compositions of mineral phases were determined using a CAMECA SX-100 electron microprobe (EMP) housed at the University of Tennessee. Pyroxene, olivine, and oxide phases were analyzed with a 1–2 μm beam size, a 20 nA beam current, and an accelerating potential of 15 kV. Maskelynite, phosphate, and sulfide compositions were measured using a 5 μm beam size, a 10 nA beam current, and an accelerating voltage between 10 kV and 15 kV. Counting times for all elements were generally 20–30 s with the exception of Y in phosphate, which was measured for 40 s. Standard PAP corrections were applied to all analyses. Precision and accuracy were monitored with natural and synthetic standards at intervals during each analytical session, and drift was within counting error. Detection limits (3σ above background) are typically <0.03 wt% for SiO_2, TiO_2, Al_2O_3, MgO, CaO, and <0.04–0.1 wt% for FeO, MnO, Cr_2O_3, NiO, Na_2O, K_2O, SO_2, P_2O_5, Y_2O_3 and V_2O_3.

2.2. Whole rock analysis

The NIPR provided a 0.160 g powdered sub-sample (Y 984028, 21) from the interior portion of the meteorite (free of cutting surfaces) for trace-element and radiogenic isotopic studies, and an additional 0.023 g aliquant of saw-dust generated during curation of Y 984028.

2.2.1. Major-element composition

About 10 mg of saw-dust (Y 984028, 91) from a single cutting surface through the meteorite was

fused in a N_2 atmosphere, using a Mo-strip heater, and quenched to form a glass bead. Major-element compositions of this bulk-rock sample were determined by electron microprobe analyses on the glass bead ($n = 35$) using a 10 μm beam size, 10 nA beam current, and an accelerating voltage of 15 kV. Loss of volatile elements (e.g., Na, K, P) is thought to be minimal during the short fusion time (~20 s) of fused bead creation, particularly in Mg-rich samples similar to Y 984028. In addition, it is possible that a small amount of Fe may be lost during bead formation due to interaction with the Mo-strip (Brown, 1977; Beck et al., 2009), but this is thought to be within the 1 σ_{stdev} value of the results. Major-element compositions of geochemical reference materials generally compare well with those determined by different methods that necessitate larger sample aliquots (Brown, 1977). Procedural blanks associated with the Mo-strip heating method have not been determined during this analysis, but in contrast to some alternative methods of constraining major-element concentrations no flux is added to the sample powder.

2.2.2. Minor and trace-element abundances

Minor- and trace-element analyses were performed on the fused glass bead using a New Wave Research UP213 (213 nm) laser-ablation system, coupled to a ThermoFinnigan Element 2 ICP-MS, at the University of Maryland. Analyses were performed via continuous rastering of the bead generating 40–80 μm wide pits with 1–2 μm deep trenches. A laser repetition rate of 7 Hz and a photon fluence of 2.5 J/cm^2 were employed for all analyses. The NIST 610 glass standard was used for calibration purposes, and the BCR-2g glass standard was analyzed as an unknown to assess accuracy and reproducibility (Table 4). Minor- and trace-element reproducibility of the standard was better than 5% (relative standard deviation; RSD), with the exception of Tm (6%), Er (6%), Ta (7%), and Gd (8%). Elemental abundances of BCR-2g were generally within error (1 σ_{stdev}) of the accepted value, with the exception of Rb, Y, Zr, Ba, La, Pr, Nd, Sm, Tb, Ta and U that were within 2 σ_{stdev} of the accepted value, and Nb, Ta, Th and Pb that were within 4 σ_{stdev} of the accepted value. LA-ICP-MS analyses were normalized to the CaO value of the glass bead as determined by microprobe analysis. Measurement of multiple analytical points ($n = 35$) during major-element analyses, and rastering during trace-element analyses indicate good bead homogeneity (shown by the 1 σ_{stdev} values given in Tables 3 and 4). Minor-elements such as siderophile Mo and W may have experienced contamination from the Mo-strip, therefore these element abundances are not reported for the glass-bead.

2.2.3. Oxygen isotopic composition

Oxygen isotope ratios were measured at the Geophysical Laboratory, Carnegie Institution of Washington using the procedure of Rumble and Hoering (1994). Reported values are given as $\delta^{18}O$, $\delta^{17}O$, and $\Delta^{17}O$. The δ values describe the per mil (‰) deviation from the international standard, V-SMOW:

$$\delta^{X}O_n = [1000 \times (({}^{X}O/{}^{16}O_n)/({}^{X}O/{}^{16}O_{std})) - 1],$$
$$\text{where } X = 18 \text{ or } 17.$$

The deviation from the terrestrial fractionation line is described as:

$$\Delta^{17}O = 1000\ln((\delta^{17}O/1000) + 1) - \lambda \times 1000\ln((\delta^{18}O/1000) + 1),$$
$$\text{where } \lambda = 0.526.$$

Prior to oxygen isotope analysis, 1.47 mg of Y 984028 powder (from the saw-dust) was ultra-sonicated in dilute hydrochloric acid and magnetic material was removed with a hand magnet. Samples were loaded in a Sharp-type reaction chamber (Sharp, 1990). Successive, repeated blanks were carried out for 12 h until there was <150 μm non-condensable gas pressure remaining after a blank run. Quantitative release of oxygen by fluorination reaction was performed by heating samples individually with a CO_2 laser in the presence of BrF_5. Standardization of oxygen isotopic values was achieved by comparison with the Gore Mountain garnet (USNM 107144), which was analyzed during each analytical session.

2.2.4. Highly siderophile element abundances and Re–Os isotopic systematics

Highly-siderophile element (HSE) abundances and Re–Os isotope measurements were performed at the University of Maryland on 75 mg of Y 984028, 21 sample powder. Digestion and spike equilibration were achieved by the addition of 3 mL of concentrated HNO_3, 2 mL of concentrated HCl, and appropriate amounts of mixed ^{185}Re–^{190}Os and HSE (^{99}Ru, ^{105}Pd, ^{191}Ir, ^{194}Pt) spikes that were sealed in a pre-cleaned, chilled 12 mL Pyrex borosilicate Carius tube and heated to 270 °C for 96 h. Osmium was extracted from the acid solution by CCl_4 solvent extraction (Cohen and Waters, 1996), then back-extracted into HBr, followed by purification by means of a micro-distillation procedure (Birck et al., 1997). Ru, Pd, Re, Ir, and Pt

were separated and purified using anion-exchange chromatography.

Osmium isotope measurements were accomplished by negative thermal-ionization mass-spectrometry (NTIMS: Creaser et al., 1991) using an electron multiplier detector of the NBS mass-spectrometer at the *Isotope Geochemistry Laboratory* (*IGL*), University of Maryland. The measured isotope ratios were corrected for mass fractionation using $^{192}Os/^{188}Os = 3.083$. The $^{187}Os/^{188}Os$ ratio of 3.5 pg loads of the in-house Johnson–Matthey Os standard, measured during the period of the data collection averaged 0.11383 ± 0.00021 ($N = 9$, 2 σ_{stdev}).

The measurements of all other HSE were performed at the *IGL* by multi-collector inductively coupled-plasma mass-spectrometry (MC-ICP-MS), using a *Nu Plasma* instrument with a triple-electron-multiplier configuration in static mode. Isotopic mass fractionation was monitored and corrected for by inter-spersal of samples with standards. The accuracy of the data was assessed by comparing the results for the reference materials UB-N and GP-13 run with Y 984028 with results obtained in other laboratories (*c.f.,* Table 1 of Puchtel et al., 2008a). Generally, concentrations of all the HSE and the measured Os isotope compositions obtained at the *IGL* are in good agreement with values reported for UB-N and GP-13 by other laboratories. The spikes and analytical techniques used in this study were the same as those used for generating the HSE database for chondrites (Walker et al., 2002; Horan et al., 2003). Diluted spiked aliquots of iron meteorites were run during each analytical session as secondary standards. The results from these runs agreed within 0.5% for Ir, 0.8% for Re, and 2% for Ru, Pt, and Pd with fractionation-corrected values obtained from measurements of undiluted iron meteorite samples, using Faraday cups of the same instrument with a signal of >100 mV for the minor isotopes.

The total analytical blanks (pg) were: Ru = 0.58, Pd = 6.5, Re = 0.20, Os = 0.11, Ir = 0.22, and Pt = 1.3. In the case of Os, Ir, and Ru, the blanks, on average, constitute less than 0.2% of the total element analyzed, and the precision of the concentration data is conservatively estimated to be better than 0.2% for Os, and 1% for Ir and Ru. The Re, Pt, and Pd blanks, on average, constitute less than 3%, 0.6%, and 5%, respectively, of the total element analyzed. The precision of the Re, Pt, and Pd concentration data is conservatively estimated to be better than 1.5%, 1.0%, and 2.5%, respectively, assuming a 50% variation in the blank. The uncertainty in the Re concentration is the main source of error on the Re/Os ratio.

Table 1
Modal Abundance in Zones A, B, and C.

	Zone A	Zone B	Zone C
Olivine	25	61	27
Pyroxene	72	17	2
Maskelynite	<1	10	–
Chromite	3	4	4
Ilmenite	–	1	–
Sulfide	<1	<1	–
Merrillite	–	2	–
FG matrix	–	–	65
Impact melt	–	5	2

Modes in Zones A, B and C of Y 984028, 51–3 are given as volume % and were determined from the processing of a BSE-image and compositional X-ray maps utilizing Image-J software. FG = fine-grained. Errors associated with image processing are estimated to be 1–5% (2 σ_{stdev}) of the measured modal abundances, and are a function of the image resolution and grey-scale contrast. The modal abundance of Zone D was not determined as we were unable to acquire an image of suitable resolution to distinguish microlite modes.

3. Results

3.1. Petrographic characteristics

The polished section of Y 984028 that we studied consists of three coarse-grained textural zones and a partially devitrified fusion crust (Fig. 1; Table 1). Two of the three identified textural zones – the poikilitic (Zone A), and non-poikilitic (Zone B) - are similar to those identified in other lherzolitic shergottites (e.g., Lewis Cliff [LEW] 88516; Alan Hills [ALHA] 77005; Y 000027; Y 000047; Y 000097; Treiman et al., 1994; Mikouchi and Kurihara, 2008). An important aspect of the mini-consortium study of this meteorite is the recognition that different sections of Y 984028 contain different proportions of poikilitic and non-poikilitic lithologies (Hu et al., 2009; Mikouchi et al., 2009), likely as a consequence of the coarse-grain sizes (>0.5 mm) and the heterogeneous distribution of textural zones. We have also identified an unusual brecciated zone (Zone C) in Y 984028. In addition, there is a partially devitrified fusion crust on this meteorite (Zone D).

Approximately 40% of the section we studied is composed of a single, twinned pyroxene oikocryst (Zone A; 1.5 by 3 mm), enclosing subhedral olivine (300–750 μm at the long axis), euhedral chromite (20–70 μm), with rare troilite (5–15 μm) and traces of maskelynite (~75 μm) at the rim. Enclosed olivines themselves contain chromite inclusions (<20 μm; Fig. 2A); chromite also occurs as individual crystals, and clusters within the pyroxene oikocryst (Fig. 1). A

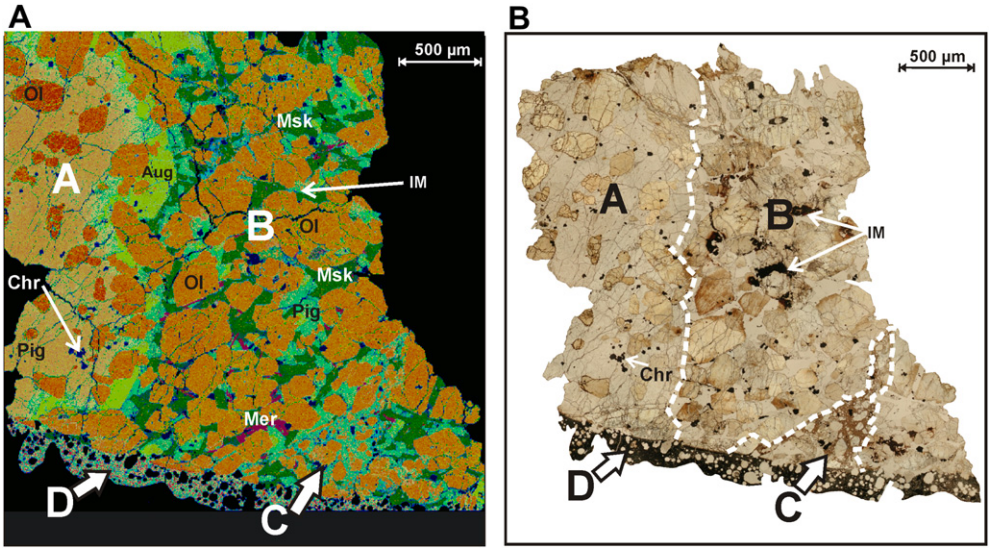

Fig. 1. A: Combined MgKα–CaKα map of Y 984028, 51–3. B: Transmitted light image of Y 984028, 51–3. Different lithologies (A, B, C) are labeled. A = poikilitic zone; B = non-poikiltic zone; C = breccia zone; and Zone D = fusion crust. Aug = augite. Chr = chromite. Msk = maskelynite. Mer = merrillite. IM = impact melt. Ol = olivine (dark red olivine has high Mg). Pig = pigeonite. (For interpretation of the references to colour in this figure legend, the reader is referred to the web version of this article.)

relatively small portion of Zone A is separated from the main oikocryst by a narrow crack (Fig. 1) containing some angular pyroxene and olivine fragments (<15 μm).

Zone B is comprised of euhedral–subhedral olivine (200–700 μm at the long-axis), and intercumulus pyroxene and maskelynite. Euhedral chromites (5–15 μm) occur both as inclusions in olivine and as individual interstitial grains. Minor troilite (5–20 μm), ilmenite, and merrillite (all up to 300 μm in length) are often closely related and occur as interstitial phases. Zone B contains localized impact-melt pockets (<300 μm) that contain lithic fragments (<75 μm) resulting from incomplete melting of local crystals (Fig. 2D). Other sections of Y 984028 contain melt veins up to 400 μm in width (Hu et al., 2009; Mikouchi et al., 2009) that appear to be bounded by the different internal textural zones in one case (Mikouchi et al., 2009). In both Zones A and B, olivines commonly have a brown coloration and can contain devitrified melt inclusions (Figs. 1B and 2C). These devitrified melt-inclusions contain occasional pyrrhotite, maskelynite, chromite, and ilmenite crystals (2–20 μm). Many melt inclusions are encircled by a narrow (<20 μm) halo of low-Ca pyroxene.

Zone C is a breccia that accounts for ~15% of Y 984028, 51–3. Angular olivine (20–200 μm), occasional pyroxene (<100 μm), and Ti-chromite (generally <20 μm) occur as poorly sorted fragments within a fine-grained matrix (Figs. 1 and 2F). The largest Ti-chromite crystal in Y 984028, 51–3 occurs in Zone C (150 μm; Fig. 2F). Some olivine crystals in Zone C have a topotactic recrystallization texture (Fig. 2B). Cross-cutting relationships between the magmatic textural zones, the breccia zone, and the fusion crust show that Zone C formed after magmatic crystallization, but prior to Earth entry. The breccia is petrographically distinct from black glassy patches associated with impact melting, but is similar to a narrow breccia (75 μm) adjacent to the small, dislocated portion of Zone A. To date, the only similar texture reported in other lherzolitic shergottites was identified in Y 793605, where a similar lithology was referred to as a "shock-induced crushed zone" by Ikeda (1997).

Evidence of shock-induced metamorphism in Y 984028 is abundant and includes pervasive fractures throughout this sample, maskelynite formation, undulatory extinction in pyroxene, mosaicism of olivine, topotactic recrystallization textures of olivine in Zone C, impact-melt pockets up to 300 μm in maximum dimension (concentrated in Zone B), and 400 μm wide melt veins reported in some other sections of this meteorite (e.g., Hu et al., 2009; Mikouchi et al., 2009). The brown olivines in this sample are similar to those reported for other martian meteorites (see Basu Sarbadhikari et al., 2009, for a discussion), and may be associated with oxidation during impact (Ostertag et al., 1984). Fractures do not

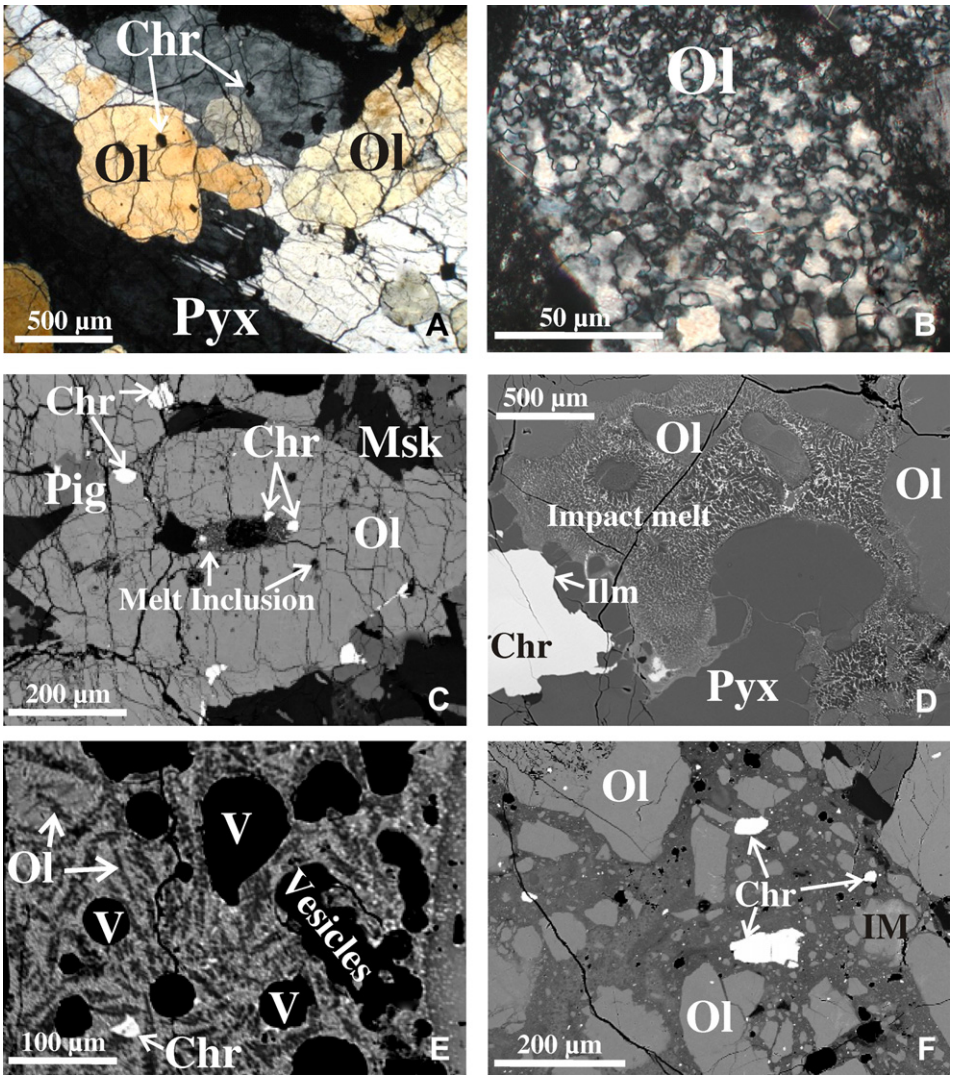

Fig. 2. Petrographic features in Y 984028, 51−3. Chromite = Chr; Ilmenite = Ilm; Impact melt = IM; Maskelynite = Msk; Olivine = Ol; Pigeonite = Pig; Pyroxene = Pyx; Vesicles = V. Images A and B are taken in cross-polarized light, and those shown in C−F are back-scattered electron (BSE) images. A: Olivine grains ± chromite enclosed within the pyroxene oikocryst that has a partially faulted twin plane. B: Olivine with topotactic recrystallization texture in Zone C. C: Large euhedral olivine in Zone B containing a large central melt inclusion and numerous smaller melt inclusions. All melt inclusions are devitrified. D: Impact melt adjacent to olivine, low Ca-pyroxene, and chromite in Zone B. The impact melt contains partially digested olivine fragments. E: Fusion crust with dendritic olivine laths, vesicles, and a single chromite crystal. F: Portion of the Zone C breccia containing angular olivine and chromite fragments.

cross-cut the breccia, but some small and discontinuous fractures are present within more clast-rich sections of Zone C, and are oblique to the elongation and boundaries of this zone. Fractures within Zones A and B are generally narrow (<2 µm), and do not greatly displace the minerals that they cross-cut. The fractures have multiple orientation directions, which are often oblique to the orientation of Zone C. Adjacent to small impact melts, fractures are less common suggesting that stress is locally accommodated by melting rather than brittle fracturing. Based upon the degree of strain recorded by olivine, the conversion of feldspar to maskelynite, and the occurrence of impact-melt veins, this is a strongly shocked sample that experienced shock pressures of 45−55 GPa, and post-shock temperatures of 600−850 °C (following Stöffler et al., 1991). Zones A, B, and C contain minor quantities of secondary Fe-hydroxide (<<1 vol%) along grain boundaries close to narrow cracks that cross-cut the sample.

The fusion crust (Zone D) of Y 984028 is partially devitrified, vesicular, and consists of numerous

dendritic olivines (10–100 μm in length), microlites of pyroxene, and minor chromite grains (Fig. 2E). It is similar to, although more vesicular than, the fusion crust of NWA 1950, which is also partially devitrified (*c.f.,* Fig. 2d of Gillet et al., 2005).

3.2. Mineral chemistry

3.2.1. Pyroxene

The pyroxene oikocryst in Zone A is chemically zoned from core ($Wo_{3-7}En_{76-71}$) to rim ($Wo_{33-36}En_{52-49}$) (Fig. 3, Table 2). Similar compositional zoning in pyroxene oikocrysts has been reported in other sections of Y 984028, and augite "patches" within the oikocryst associated with maskelynite inclusions have also been observed (Hu et al., 2009). Inter-cumulus pigeonite and augite in Zone B are more Fe, Ca, Ti, and Al-rich ($Wo_{7-37}En_{67-47}$) than the oikocryst, and are irregularly zoned (Fig. 3). Pyroxene compositions in the poikilitic (Zone A) and non-poikilitic (Zone B) areas coincide with the range of Wo-contents reported for other sections of Y 984028 (Hu et al., 2009; Mikouchi et al., 2009), but reach lower absolute Wo-contents than these authors observed (Wo <3; Table 2). Pyroxene compositions in Y 984028 overlap the range observed in other lherzolitic shergottites (e.g., Grove Mountains [GRV] 99027, ALHA 77005, LEW 88516, Y 793605, and Y 000027/000047/000097; Fig. 3). Equilibration temperatures from two-pyroxene thermometry were obtained using the QUILF program (Anderson et al., 1993) and are ~1100 °C at the oikocryst rim, with similar values calculated in irregularly zoned interstitial pyroxenes of Zone B (~1020 °C). The calculated temperatures for Y 984028 pyroxenes are similar to those determined in, LEW 88516, Y 793605, ALHA 77005, GRV 99027, and in Y 000027/000047/000097 (~1000–1200 °C; Meyer, 2009). The slope defined by a zero-intercept regression line through the Mn/Fe values in the constituent pyroxenes of Y 984028 (not shown) overlaps the range of compositions that define the martian planetary trend given by Papike et al. (2003, 2009).

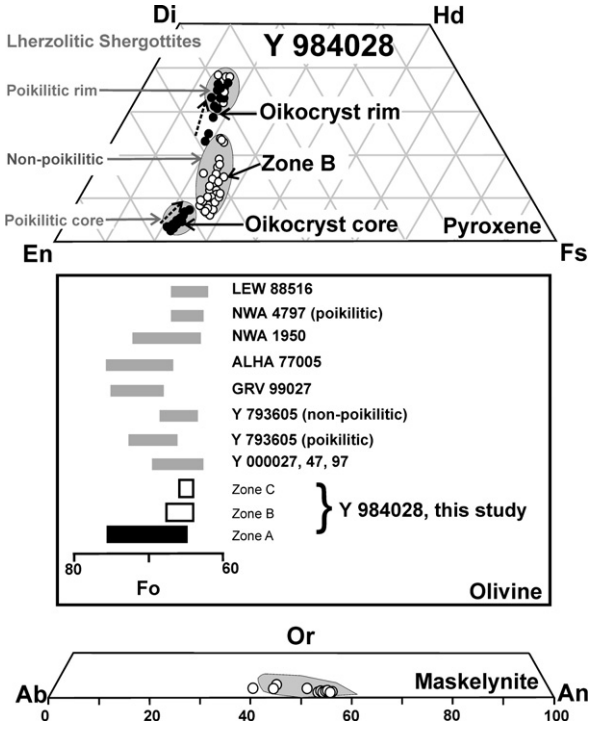

Fig. 3. Compositions of silicate minerals in Y 984028, 51-3. Filled symbols correspond to the zone A, open symbols refer to zone B, and zone C. The black arrow marks increasing amounts of diopside in the oikocryst rim. Literature data for the compositions of pyroxene and maskelynite in Y 793605, LEW 88516, ALHA 77005, GRV 99027, NWA 1950, NWA 4797, and Y 000027/000047/000097 are shown as grey fields (Meyer, 2009).

3.2.2. Olivine

Individual olivine crystals are homogeneous, but inter-grain variations range from Fo_{74} to Fo_{66} (Fig. 3, Table 2). High-Mg olivines (Fo_{74-70}) occur in the core of the pyroxene oikocryst, whereas those at the oikocryst rim have higher Fe-contents (Fo_{69-68}), overlapping the range of the olivine compositions in Zones B and C (Fo_{68-66}). Olivine compositions in Zones A and B coincide with reported olivine compositions from poikilitic, and non-poikilitic zones in other sections of Y 984028 (Hu et al., 2009; Mikouchi et al., 2009), and are similar to olivine compositions in poikilitic and non-poikilitic areas of other lherzolitic shergottites (Y 793605, GRV 99027, ALHA 77005, and Y 000027/000047/000097; Fig. 3). However, these olivine compositions do not extend as low as the Mg concentrations observed in olivine crystals of LEW 88516 (Fo_{64}; Treiman et al., 1994). The Mn/Fe values of Y 984028 olivines coincide with those in other lherzolitic shergottites and the martian olivine Mn–Fe fractionation trend given by Papike et al. (2003, 2009).

3.2.3. Maskelynite and other phases

Maskelynite crystals are rare in Zone A, but are common as an interstitial phase in Zone B. Maskelynites are irregularly zoned from An_{55} to An_{39}. Hu et al. (2009) and Mikouchi et al. (2009) reported a wider range of maskelynite compositions (An_{57-33}) than we observed in our section. Chromite grains

Table 2
Representative mineral compositions in Y 984028, 51−3.

	Pyroxene				Olivine					Chromite		Ilm	Merr	Msk	Zone D			Impact Melt		Tr
	Zone A core	Zone A rim	Zone B 1.	Zone B 2.	Zone A core	Zone A rim	Zone B	Zone C	Zone D	Zone A	Zone B	Zone B	Zone B	Zone B.	1.	2.	3.	I	II	Zone B
SiO_2	55.4	52.3	51.6	53.3	38.1	37.3	37.0	36.8	41.3	0.14	0.04	0.05	0.10	57.7	49.4	49.8	44.9	55.8	37.2	
TiO_2	0.10	0.42	1.28	0.44						1.24	14.0	53.0			0.77	0.71	0.44	1.45	<0.03	
Al_2O_3	0.36	1.70	1.47	0.43					0.09	6.60	5.33	<0.03		26.5	4.11	4.29	3.10	15.4	<0.03	
FeO	14.5	9.23	9.77	17.9	22.8	26.8	28.6	28.4	7.72	23.9	39.0	38.4	0.84	0.28	17.7	20.4	21.2	4.93	29.0	
[a]Fe_2O_3										3.2	5.13									
MnO	0.45	0.41	0.38	0.61	0.49	0.56	0.54	0.56	0.30	0.48	0.68	0.75	0.69			0.63	0.50	0.11	0.66	
CaO	1.31	17.4	18.0	2.99	0.17	0.21	0.19	0.26	0.17			0.13	47.5	8.72	8.25	8.44	4.24	14.9	0.33	
MgO	28.1	17.1	16.2	23.7	37.7	34.2	33.1	33.2	49.5	6.19	3.54	5.34	3.57	0.08	16.0	12.5	22.4	3.22	33.5	
Na_2O	<0.04	0.22	0.31	0.06									1.87	5.93	0.56	0.67	0.49	1.58	<0.04	
K_2O	<0.05	<0.05	<0.05	<0.05										0.50	<0.05	<0.05	<0.05	<0.05.	<0.05	
P_2O_5													45.6		0.46	0.51	0.23	1.87	0.15	
Cr_2O_3	0.40	0.88	0.65	0.13	0.05	<0.03	<0.03	<0.03	0.41	56.7	30.8	1.15			0.22	0.17	0.39	<0.03.	<0.03	
NiO						0.06		<0.05	0.10											
SO_2																		<0.05	<0.05	
V_2O_3										0.70	0.62									
Y_2O_3													0.06							
ZrO_2												0.09								
S																				36.4
Fe																				60.2
Co																				0.14
Ni																				2.36
total	101	99.7	99.7	99.6	99.2	99.2	99.5	99.1	99.6	99.2	99.1	99.0	99.7	99.8	98.2	98.1	98.0	99.4	101	99.1
Mg#	78.1	77.8	76.0	71.1	74.7	69.5	67.4	67.6	92.0	31.6	13.9	19.9	60.1	34.7	64.1	54.8	67.6	27.2	69.6	
End Members																				
Wo	2.54	35.9	37.4	5.98																
En	75.6	49.2	46.8	66.0																
Fs	21.8	14.9	15.8	28.0																
Fo					74.1	68.8	66.8	66.8	91.4											
Fa					25.1	30.2	32.4	32.1	8.00											
Te					0.55	0.65	0.60	0.65	0.36											
Ca-Ol					0.24	0.30	0.25	0.40	0.23											

Oxide contents are given as wt% values, end member compositions are given as molar%. Mg# = 100 × Mg/(Mg + Fe^{2+}), Ilm = ilmenite; Merr = merrillite, Msk = maskelynite, Tr = troilite. Fusion crust (Zone D) compositions 1, 2, and 3 correspond to the glassy matrix ~200 μm from the substrate contact with zones A, B and C respectively. A more extensive catalogue of mineral compositions is provided in the supplementary online material (SOM) accompanying this publication. End-member compositions are calculated from cation values derived from site-balance calculations (SOM).

[a] The proportion of Fe^{3+} in chromite grains is calculated from cation values derived from charge balance calculations (SOM).

within the poikilitic lithology (Zone A) have higher Cr and lower Ti and Fe^{3+} contents compared to those in Zones B, and C (Fig. 4), which agree with the observations of Hu et al. (2009) and Mikouchi et al. (2009). All analyzed sulfide phases are troilite and have variable Ni-contents ranging from 1.27 to 4.49 wt%. High Ni-contents in troilite coincide with maximum values reported in several lherzolitic shergottites (reviewed in Meyer, 2009). Merrillite grains are rich in rare-earth elements (REE; up to 0.24 wt% Y_2O_3), and they are the main REE host-phase within this meteorite. Ilmenite crystals contain 3.5–5.4 wt% MgO, and have compositions similar to those reported in other lherzolitic shergottites (Table 2; Meyer, 2009). Hu et al. (2009) also reported a few baddeleyite crystals coexisting with ilmenite in non-poikilitic areas but these are not observed in Y 984028, 51–3.

3.3. Composition of melt inclusions, impact melts, and fusion crust

Melt inclusions are common in olivine crystals in Zones A and B, reaching up to 350 μm in diameter. Rare melt inclusions are present in chromite grains within the pyroxene oikocryst (<10 μm; Hu et al., 2009). All melt inclusions are devitrified to chromite, maskelynite, pyrrhotite, and minor pigeonite. Analyzed sulfide, chromite, ilmenite, and maskelynite in melt inclusions have compositions that are similar to those in Zone B. Kaersutite crystals have not been observed in the melt inclusions within Y 984028, 51–3, but are present in other lherzolitic shergottites (e.g., ALHA 77005; Ikeda, 1998). Melt inclusions are typically surrounded by narrow (<20 μm) low-Ca pyroxene halos similar to those observed in ALHA 77005 (Ikeda, 1998; Stockstill et al., 2001; Zipfel and Goodrich, 2001; Calvin and Rutherford, 2008), and Y 000027/000047/000097 (Mikouchi and Kurihara, 2008). Melt inclusions are often at the center of radial cracks, and are connected to cracks (<70 μm) that extend to crystal edges.

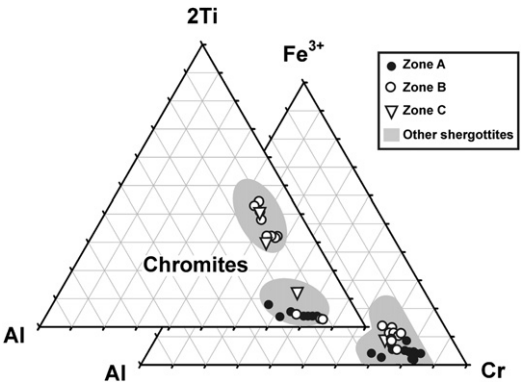

Fig. 4. Chromite composition in Y 984028, 51–3. Cation contents are calculated from charge-balance calculations. Literature data corresponds to the composition of spinel phases reported for Y 793605, LEW 88516, ALHA 77005, GRV 99027, NWA 1950, NWA 4797, and Y 000027/000047/000097 (Meyer, 2009).

Impact-melt pockets in Y 984028 are typically black and glassy in appearance, and vary in composition (Table 2). In addition, impact-melts commonly contain lithic clasts (Fig. 2D). The composition of the fusion crust (Zone D) is variable (Tables 2), and dendritic olivines (<10–100 μm) in the fusion crust are Mg-rich (Fo_{81-91}). The fusion-crust composition varies parallel to the boundary with the underlying sample, and these variations relate to the substrate mineralogy of the adjacent zone, which is similar to observations reported by Day et al. (2006a), Brandstätter et al. (2008), and Thaisen and Taylor (2009). Minerals in Zones A, B and C that are within 500 μm of the fusion crust show some evidence of modification, including discoloration, weakening of crystal form, and a small degree of partial melting.

3.4. Whole-rock chemistry

3.4.1. Major-Element and oxygen-isotopic composition

The bulk composition of Y 984028 is similar to other lherzolitic shergottites (Table 3). Although the bulk-composition of Y 984028 is determined from a small powder aliquot (10 mg) derived from a single cutting plane, major-element concentrations and inter-element abundances are generally within error of the average major-element values reported for other lherzolitic shergottites. This observation suggests that the major-element composition reported here provides a reasonable representation of the bulk-rock. In detail, the bulk composition of Y 984028 closely resembles average values of Y 793605, ALHA 77005, and LEW 88516. Oxygen isotopes in Y 984028, 91 place this sample within the range of other shergottites and confirm its martian heritage (Fig. 5, Table 3). In particular, $\Delta^{17}O$ in this sample lies below the average value of martian mass-independent oxygen isotopic fractionation (e.g., Franchi et al., 1999; Rumble and Irving, 2009), and is similar to NWA 4767 and ALHA 77005. Low $\Delta^{17}O$ has been linked to Antarctic weathering (Misawa et al., 2009), although the acid-wash prior to oxygen analysis was utilized to eliminate products of terrestrial weathering (Rumble and Irving, 2009) and the low $\Delta^{17}O$ observed here may be a magmatic signature inherited on Mars.

Table 3
Major-element, oxygen isotope, and Re–Os isotope compositions in Y 984028 and other lherzolitic shergottites.

	Y 984028	Y 793605	NWA 4797	LEW 88516	NWA 1950	ALHA 77005
SiO_2 (wt%)	43.9 (2)	45.4	41.6	46.2	44.0	42.6
TiO_2	0.32 (3)	0.29	0.40	0.37	0.55	0.47
Al_2O_3	3.83(1)	1.93	3.70	2.88	4.02	2.83
FeO	18.3(4)	19.2	19.8	19.5	21.7	19.8
MnO	0.49(2)	0.51	0.50	0.49	0.49	0.46
CaO	4.83(2)	3.93	4.70	4.32	4.61	3.29
MgO	27.1(4)	26.7	25.6	24.6	22.9	27.8
Na_2O	0.30(2)	0.30	0.55	0.51	0.82	0.46
K_2O	<0.05	<0.02	0.10	0.10	0.06	<0.03
P_2O_5	0.22(4)		0.40	0.39	0.68	0.36
Cr_2O_3	0.95(7)	1.07	1.01	0.88	0.97	1.01
SO_2	0.07(2)					
Mg#	72.5	71.3	69.7	69.2	65.3	71.5
Total	100.34	99.3	98.3	100	99.1	98.8
$\Delta^{17}O$ (‰)	0.218	0.21	0.274	0.26	0.312	0.16
$\delta^{17}O$	2.24	2.30	2.148	2.39	2.54	2.15
$\delta^{18}O$	3.84	4.01	3.564	4.14	4.28	3.85
Os (ppb)	3.264	1.017		0.905		3.405
Ir	2.250			1.291		3.366
Ru	3.437			2.413		4.386
Pt	2.811			2.559		2.130
Pd	1.621			1.636		1.319
Re	0.0816	0.277		0.0222		0.256
$^{187}Re/^{188}Os$	0.120(2)	0.12(4)		0.131(4)		0.363(4)
$^{187}Os/^{188}Os$	0.1284(2)	0.1336(4)		0.1316(2)		0.1324(3)
Crystallization Age (Ma)	170 ± 9	173 ± 14		183 ± 10		185 ± 11
$^{187}Os/^{188}Os_i$	0.1281(2)	0.1306(4)		0.1285(2)		0.1312(2)
$^{87}Sr/^{86}Sr_i$	0.71039(3)	0.71042(7)		0.71052(4)		0.71026(4)

The bulk-rock compositions of other lherzolitic shergottites are obtained from Brandon et al. (2000), Meyer (2009), and Puchtel et al. (2008b). The composition of Y 984028 is obtained by replicate analyses of a fused glass-bead ($n = 35$), errors denoted by (x) are the variance in terms of the least decimal cited, and correspond to $1\sigma_{stdev}$ of the major-element compositions, and 2 σ (standard error) of the measured Re–Os isotopic compositions and initial osmium isotope values. Crystallization ages and initial $^{87}Sr/^{86}Sr$ values are from Borg et al. (2002), Morikawa et al. (2001) and Shih et al. (2009). All oxides are reported as wt%, Mg# = Mg/(Mg + Fe) × 100.

3.4.2. Trace-element characteristics

Y 984028 is LREE-depleted ($[La/Sm]_n = 0.47$, $[La/Yb]_n = 0.39$; where n denotes normalization to CI-chondrite; Fig. 6). La/Sm and La/Yb values plot in the range of the intermediate shergottite group and are significantly higher than values in strongly-depleted shergottites. Rb, Sr, Sm, and Nd contents in Y 984028, 91 are within error of those reported for a different powder aliquot of this same meteorite measured by Shih et al. (2009). The REE abundances of Y 984028 are also within uncertainty of those reported for lherzolitic shergottites ALHA 77005, LEW 88516, and Y 000097 (Fig. 6A, Table 4). Lherzolitic shergottite NWA 1950, and intermediate shergottite EETA 79001 (portions A and B) have similar REE profiles, but higher absolute REE abundances when compared with Y 984028; Y 793605 also has a similar REE profile, but lower REE abundances, compared with Y 984028. The extended trace-element plot (Fig. 6B) shows elevated Zr_n and Hf_n relative to Nd_n and Sm_n, and Rb_n depletion relative to

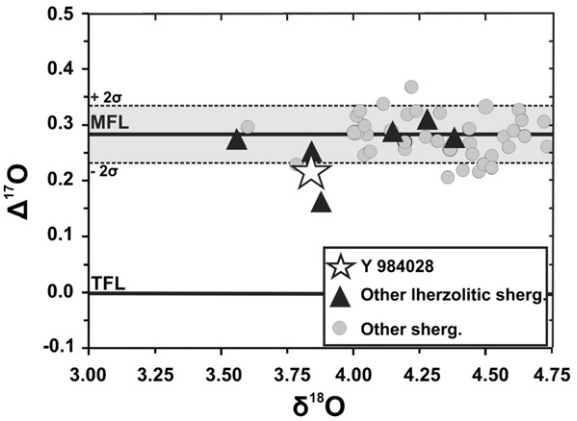

Fig. 5. Bulk rock oxygen isotopic composition of Y 984028. MFL = martian fractionation line; sherg = shergottite; TFL = terrestrial fractionation line. Literature data are from Meyer (2009) and a compilation by Rumble and Irving (2009).

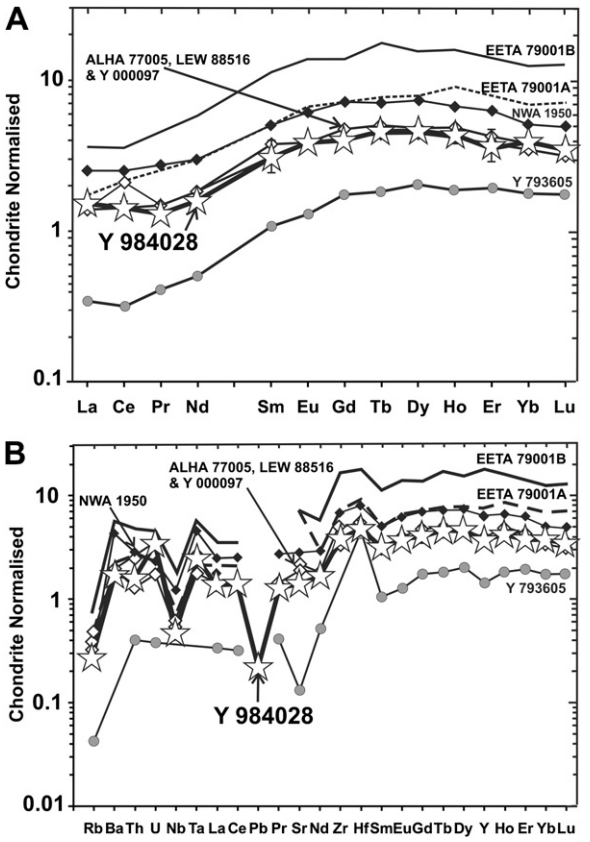

Fig. 6. Rare-earth-element (A) and extended trace-element (B) compositions of Y 984028, other lherzolitic shergottites, ALHA 77005, LEW 88516, NWA 1950 and Y 793605, and lithology A and B of basaltic shergottite EETA 79001 (black lines; Meyer, 2009). All values are normalized to the CI-chondrite value estimate of Anders and Grevesse (1989). Error bars shown for analysis of Y 984028 are given at the 2σstdev level.

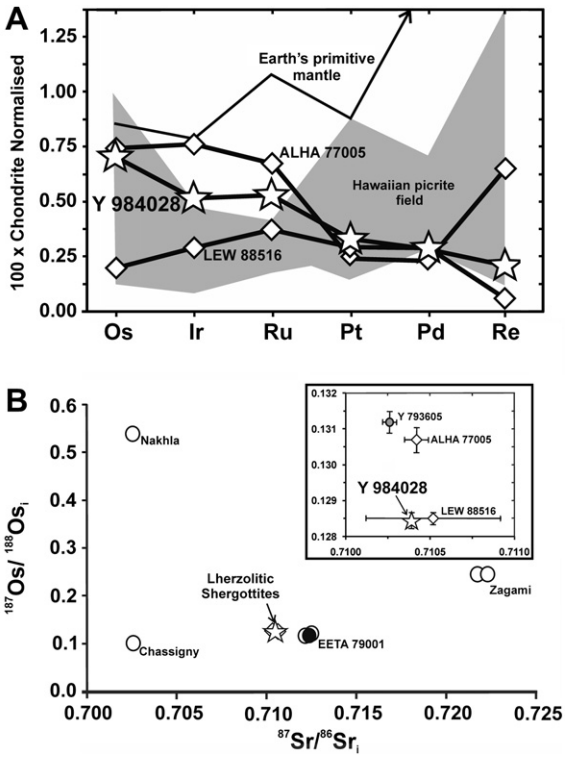

Fig. 7. A: Bulk-rock highly-siderophile element contents of lherzolitic shergottites (this study, Puchtel et al., 2008b) are normalized to the value of Orgueil (Horan et al., 2003) and multiplied by 100. The dark grey field marks the highly-siderophile element composition of Hawaiian picrites (Ireland et al., 2009). The composition of Earth's primitive mantle is from Becker et al. (2006), and Pd and Re abundances estimated by these authors plot at values greater than the scale shown. B: Bulk-rock initial $^{87}Sr/^{86}Sr$ values with corresponding $^{187}Os/^{188}Os$ values calculated at the time of crystallization age. The inset shows the values reported in lherzolitic shergottites (filled circles). The white-star marks the composition of Y 984028. Initial Sr isotope ratios are derived from internal mineral correlations given in Gale et al. (1975), Nakamura et al. (1982), Wooden et al. (1982), Morikawa et al. (2001), Nyquist et al. (2001, 2006), Borg et al. (2002), Misawa et al. (2008), and Shih et al. (2009). The initial osmium isotopic value of EETA 79001 was determined for a three point correlation (Brandon et al., 2008). For all other samples $^{187}Os/^{188}Os$ values are calculated from the Re–Os isotopic compositions reported by Brandon et al. (2000) and corrected to the age defined by the Rb–Sr isotope characteristics.

Ba_n in Y 984028; similar inter-element fractionation is a common characteristic of most martian meteorites (*c.f.,* Meyer, 2009). Although current data indicate that trace-element concentrations of Y 984028 are reproducible, trace-element abundances may be variable between different whole-rock powder aliquots, and Shirai and Ebihara (2009) suggested that this typically reflects inhomogeneity in small powder fractions (~20 mg) especially in course-grained samples such as Y 984028. Additionally, these authors indicated that some systematic differences may be evident when trace-element abundances are determined by different analytical techniques. However, inter-element ratios are similar within the lherzolitic shergottite group suggesting that whereas absolute concentrations may vary as a result of sample heterogeneity, many trace-element ratios are not significantly affected.

3.4.3. Re–Os isotope systematics and highly-siderophile element abundances

Osmium, Ir, Ru, Pt, Pd, and Re contents measured for Y 984028, 21 (Fig. 7A; Table 3) are within the range of other lherzolitic shergottites (Brandon et al., 2000; Puchtel et al., 2008b). Lherzolitic shergottites have relatively high Os_n, Ir_n, and Ru_n (I-PGE) contents compared to Pt_n, Pd_n (P-PGE), and Re_n. As with other lherzolitic shergottites, the Re/Os value of this meteorite is low ($^{187}Re/^{188}Os = 0.120 \pm 0.002$), so age

correction to the time of crystallization (~170 Ma; Shih et al., 2009) is minor. The calculated initial $^{187}Os/^{188}Os$ of Y 984028 is within the range of chondritic meteorites (Table 3). The initial $^{187}Os/^{188}Os$ value (0.1281 ± 0.0002) is within uncertainty of the initial ratio determined for LEW 88516 (Brandon et al., 2000; Fig. 7B). The range of I-PGE concentrations and measured $^{187}Os/^{188}Os$ values of lherzolitic shergottites overlap I-PGE abundances and osmium isotope compositions of terrestrial picrites from Hawaii (Fig. 7 and Table 3).

4. Discussion

4.1. Significance of the Zone C breccia

The cross-cutting relationship between the Zone C breccia and the fusion crust in the studied section of Y 984028 indicates formation of Zone C before or during impact ejection from Mars (*c.f.,* regolith breccia vs. in-situ brecciation origin). Brecciated areas were not reported in other sections of Y 984028. Other petrographic studies of Y 984028 (Hu et al., 2009; Mikouchi et al., 2009), have indicated that impact-melt veins are associated with fragmented angular crystals, but melt veins are not observed in Zone C of Y 984028, 51-3. The matrix of Zone C is not glass-dominated like normal impact-melt pockets and veins (Fig. 1), nor has an impact-melt pocket equivalent in size to Zone C ever been reported in other lherzolitic shergottites. In addition, topotactic recrystallization of olivine (Fig. 2B) in Zone C was not observed in or adjacent to impact-melt pockets of Y 984028, 51-3. The textural features of this breccia may be linked to cataclastic processes during impact ejection, or may correspond to an earlier impact event on the martian surface. Given the small size of the studied portion of Y 984028 it is difficult to constrain the characteristics of the entire breccia portion of this meteorite, and further study is required.

4.2. Crystallization sequence and crystallization age

Petrographic and compositional relationships show that the crystallization sequence of Y 984028 is as follows: (Zone A) chromite → Mg-rich olivine (Fo_{74-68}) + orthopyroxene → olivine

Table 4
Bulk-rock trace-element composition of lherzolitic shergottites given in ppm.

	Y 984028	Y 793605	LEW 88516	NWA 1950	ALHA 77005	[a]BCR2g	[a]RSD (%)	[a]ΔS−R (%)
Rb	0.62(4)	0.0985	1.1	0.78	0.75	50	3.0	5.3
Ba	4.0 (3)	4.9	9.94	4.64	656	3.6		4.0
Th	0.045(5)	0.0177	0.037	0.083	6.5	1.1		7.9
U	0.028(3)	0.003	0.014	0.019	0.029	1.8	1.6	6.7
Nb	0.41(2)	0.51	1.12	0.57	10.6	2.3		19
Ta	0.039(1)	0.035	0.064	0.026	0.6	6.7		17
La	0.35(5)	0.0804	0.33	0.586	0.32	26.6	3.9	5.2
Ce	0.85(9)	0.192	1.26	1.51	0.84	52.8	2.9	1.5
Pb	0.51(2)	12.1			4.1	14		
Pr	0.11(1)	0.0362	0.24	0.13	6.5	3.7		5
Sr	11(1)	1.03	17	21.5	14.1	346	3.9	2.5
Nd	0.72(6)	0.226	0.82	1.34	0.82	29	3.4	2.5
Zr	14(1)	13	26	19.5	183	3.5		0.8
Hf	0.53(8)	0.456	0.52	0.82	0.58	5.0	1.2	2.7
Sm	0.4(1)	0.156	0.44	0.739	0.46	7.0	3.4	4.9
Eu	0.2062(4)	0.715	0.22	0.343	0.22	2.0	2.7	0.9
Gd	0.8(1)	0.338	1.37	0.92	6.4	8.2		5.5
Tb	0.16(3)	0.0659	0.16	0.261	0.18	1.1	2.2	3.1
Dy	1.08 (7)	0.489	1.08	1.77	1.16	6.4	4.1	0.4
Y	5.3(6)	2.28	5.7	9.61	6.18	34.4	2.4	5.9
Ho	0.23(2)	0.103	0.23	0.367	0.27	1.3	1.4	2.0
Er	0.6 (1)	0.305	0.984	0.66	3.5	6.2		3.4
Tm	0.08(1)	0.5			5.9	8.3		
Yb	0.61(2)	0.281	0.57	0.81	0.55	3.6	5.0	7.0
Lu	0.086(5)	0.0418	0.083	0.12	0.077	0.5	2.6	3.0

Values corresponding to Y 793605, LEW 88516, NWA 1950 and ALHA 77005 are sourced from Meyer (2009). Uncertainties on the sample measurement given as (x) are 1σstdev variance in terms of the least decimal cited.

[a] Values of the reference material (BCR-2g), the associated relative standard deviation (RSD), and deviation from the accepted value (ΔS − R = (sample/reference − 1) × 100) measured during this study.

(Fo_{72-70}) + pigeonite → augite → (Zone B) augite + olivine (Fo_{68-66}) + plagioclase (An_{55-40}) + Ti-chromite. Late-stage crystallization led to the formation of interstitial troilite, ilmenite, and merrillite (Fig. 8). The observed crystallization sequence is similar to that reported for other lherzolitic shergottites (e.g., Harvey et al., 1993; Mikouchi and Kurihara, 2008; Mikouchi and Miyamoto, 1997). On the basis of Fe–Mg exchange, olivines in Y 984028 are too Fe-rich to be in equilibrium with a melt composition equivalent to that of the bulk rock, and are too Mg-rich to be in equilibrium with adjacent pyroxenes (following the method of Roeder and Emslie, 1970; Ford et al., 1983 and Filiberto et al., 2009; Tables 2 and 3). These relationships indicate that Y 984028 is a cumulate rock, similar to other lherzolitic shergottites. Two-pyroxene thermometry indicates that concomitant with or following crystallization, Y 984028 equilibrated at ~1000–1100 °C (Section 3.2), and olivine grains were then homogenized probably during continued cooling. The radial-cracks of devitrified melt inclusions present in Zones A and B may have formed in response to sub-solidus volume change, and suggest that volatile contents in these melt inclusions may be susceptible to open-system behavior.

The $^{87}Sr/^{86}Sr$ and $^{87}Rb/^{86}Sr$ values of bulk rock and mineral separates of Y 984028 define a linear correlation that yields a broadly defined crystallization age of ~170 Ma (Shih et al., 2009). MSWD values (4.6–8.8) for two linear regressions of $^{87}Rb/^{86}Sr$ versus $^{87}Sr/^{86}Sr$ indicate that the Rb–Sr isotope system has experienced some disturbance and therefore the probability of this age having geological meaning in absolute terms is low. Shih et al. (2009) indicated that the uncertainty recorded by the MSWD values largely corresponds to modest disturbance during impact, and perhaps some small differences in initial ϵSr. The broadly defined crystallization age of ~170 Ma is within error of those determined by several independent dating techniques in LEW 88516, ALHA 77005, Y 793605, and Y 000097 (Borg et al., 2002; Morikawa et al., 2001; Misawa et al., 2008; Table 2). In particular, the crystallization age and initial $^{87}Sr/^{86}Sr$ value of Y 984028 (~0.71038; Shih et al., 2009) coincide with that determined for Y 793605 (Fig. 7B; Morikawa et al., 2001).

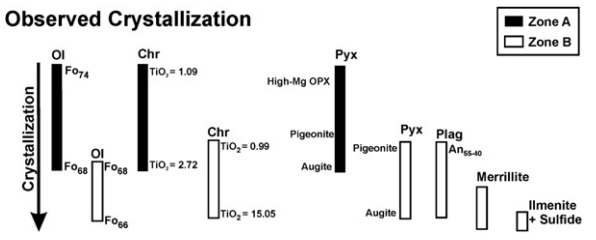

Fig. 8. Crystallization sequence of Y 984028. Chr = chromite; Ol = olivine; Plag = plagioclase; Pyx = pyroxene. The observed crystallization sequence is derived from petrographic observations.

During terrestrial atmospheric entry a partially devitrified fusion crust (Zone D) formed on Y 984028. Phases adjacent to Zone D that are discolored may represent a narrow zone that has been heated during the passage of the meteorite through the atmosphere of the Earth. Detailed descriptions of fusion crusts belonging to lherzolitic shergottites are rarely given in the literature, but those available indicate that fusion crusts are devitrified (NWA 1950; Gillet et al., 2005) like that of Y 984028. No relic phases are present in Zone D of Y 984028, 51–3, but dendritic olivines (Fo_{91-81}) and occasional chromites have crystallized from the frictional melt. Olivine compositions in the Allende fusion crust are Mg-rich, similar to those produced by an early experimental analogue of fusion crust formation (Blanchard and Cunningham, 1974). The presence of Mg-rich dendritic olivine in the fusion crust of Y 984028 indicates that the frictional melt was olivine-saturated and was above the liquidus for a relatively short period of time preventing the melt from annealing long enough to fully annihilate nucleation sites. Vesicles of Zone D may be attributed to the boiling of the frictional melt, similar to that reported from the STONE-5 experiment (Brandstätter et al., 2008). These observations suggest that meteorites experience some degassing during Earth entry and that many fusion crusts do not provide an accurate representation of the bulk-rock composition (Day et al., 2006a; Thaisen and Taylor, 2009).

4.3. Comparison with other lherzolitic shergottites

Lherzolitic shergottites, including Y 984028, have broadly similar igneous textures and mineral major-element compositions. For example, un-zoned olivines in Y 984028 are similar to those in ALHA 77005, NWA 1950, and GRV 99027, but differ somewhat from moderately zoned olivines in LEW 88516 and Y 793605 (Meyer, 2009 and references therein).

Similarities in whole-rock major-, trace-, and highly-siderophile element abundances, inter-element ratios, and osmium isotope compositions of Y 984028, and other lherzolitic shergottites ALHA 77005, LEW 88516, NWA 1950, Y 793605 and Y 000097 may indicate that they were generated by broadly similar petrogenetic processes. Furthermore, initial $^{87}Sr/^{86}Sr$ values of Y 793605, Y 000097, ALHA 77005 are within uncertainty of the initial $^{87}Sr/^{86}Sr$ composition of Y 984028 (Shih et al., 2009). The Antarctic icefield recovery sites of Y 000027, Y 000047, Y 000097, are

proximal to that of Y 984028 (Misawa et al., 2009). Therefore, we suggest that Y 984028 is compositionally paired with Y 000027, Y 000047, Y 000097.

This group of Yamato lherzolitic shergottites (Y 000027/000047/000097, and Y 984028), ALHA 77005, GRV 99027, LEW 88516, Y 793605, and NWA 1950 contain varying proportions of pyroxene oikocrysts. Samples with smaller relative volumes of pyroxene oikocrysts tend to have higher Fe and Ti contents in the constituent minerals of all textural zones, particularly in non-poikilitic regions. This has led some authors to interpret inter-sample variations in lherzolitic shergottites as a reflection of their relative position in a cumulate pile (e.g., Mikouchi and Kurihara, 2008), a situation that is broadly analogous to that described for nakhlites (e.g., Day et al., 2006b). If lherzolitic shergottites originate from a crystallizing magma with a melt of relatively uniform, but evolving composition, high-MgO samples are likely to correspond to earlier crystallization products. In this sense Y 984028, Y 000027/000047/000097, and Y 793605 with relatively high Mg, Ni, and Cr, may correspond to early crystallization products of a basaltic magma reservoir, whereas more Fe-rich LEW 88516 and NWA 1950 may represent later cumulates.

4.4. Petrogenetic constraints provided by HSE abundances and Os isotope systematics of Y 984028

The intermediate shergottite-group includes lherzolitic shergottites ($[La/Yb]_n = 0.2–0.5$ and $[Sm/Yb]_n = 0.6–1.0$) and EETA 79001 ($[La/Yb]_n = 0.2–0.3$ and $[Sm/Yb]_n = 0.7–0.9$). Petrogenetic models of intermediate shergottites can be sorted into general paradigms, including the assimilation of crustal or KREEPy (K, P, and REE-rich) materials during open-system fractional crystallization, and the generation of magma from distinct mantle sources ± metasomatism of that mantle (Herd et al., 2002; Borg and Draper, 2003; Elkins-Tanton et al., 2003; Treiman, 2003; Debaille et al., 2007, 2008; Shearer et al., 2008; Symes et al., 2008; Blinova and Herd, 2009). Here, we assess possible crustal assimilation processes acting on Y 984028, and provide some new constraints on the composition of the mantle source of lherzolitic shergottites.

It has been suggested that some lherzolitic shergottites may contain a minor crustal component, recognized in $\delta^{18}O$ variations of ~1 ‰ for the shergottite group (e.g., Day et al., 2005; Rumble and Irving, 2009; Fig. 5). Lherzolitic shergottites also show a large range of initial ϵNd values (7.8–11.7; Borg et al., 2002, 2003; Misawa et al., 2006, 2008; Morikawa et al., 2001) that may be consistent with crustal assimilation. Addition of crustal material may be of importance to the Os isotopic composition of some shergottites. However, contributions of martian crust with low Os–Ir–Ru contents (potentially analogous to the HSE inventory of terrestrial continental crust; Peucker-Ehrenbrink and Jahn, 2001, and/or constituents of the lunar crust Day et al., 2010), will lead to minor dilutional effects on the HSE composition of magmas parental to lherzolitic shergottites. These lines of evidence suggest that the contribution of martian crust may play a negligible role in modifying the Os-isotope systematics and HSE abundances of magmas parental to lherzolitic shergottites (Walker, 2009).

Alternatively, the observation of a cataclastic zone (Zone C) in Y 984028 leads to the possibility that high HSE abundances and chondritic osmium isotope compositions may be imparted by addition of meteoritic material during impact processing. However, we discount this possibility as the abundances of HSE in lherzolitic shergottites cover a relatively narrow range (0.91–3.41 ppb Os; Table 3), and do not reach concentrations typically observed in known impact melt-breccias from the moon (up to 62 ppb Os, with an average of 7.1 ± 17.9 ppb 2 σ_{stdev} Os; Puchtel et al., 2008a). In addition, Walker (2009) indicated that the observed fractionation between I-PGE and P-PGE in the shergottite suite can not be accounted for by the assimilation of high-proportions of meteoritic material. Instead, the Os-isotope and HSE characteristics of lherzolitic shergottites are likely inherited from their mantle source. Although there are few firm constraints on HSE partitioning in shergottites, bulk-rock Os abundances vary over a similar order of magnitude when compared to igneous rocks of similar MgO-content on Earth (Walker, 2009). Therefore, magmatic processes (*sensu lato*) responsible for high I-PGE concentrations and chondritic osmium isotope values observed in some high MgO terrestrial picrites (e.g., Fig. 7A) may be analogous to magmatic processes operating during the petrogenesis of lherzolitic shergottites. Therefore, the high I-PGE and modest P-PGE and Re contents of Y 984028, and other lherzolitic shergottites, may reflect the accumulation of early-formed mineral phases rich in compatible I-PGE relative to more incompatibility P-PGE.

The recent crystallization age of lherzolitic shergottites indicates that Re–Os isotope compositions have not experienced significant radiogenic in-growth since the time of melting, and provides a trace of the isotopic composition of the primary magma and mantle source. It has been suggested that the Re/Os ratio of martian

mantle reservoirs were acquired during early differentiation (Brandon et al., 2000). Assuming the Re/Os ratio of the mantle source remained undisturbed until melting to produce primary magmas from which the lherzolitic shergottites crystallized at ~170 Ma, the osmium isotopic composition of Y 984028 and other lherzolitic shergottites suggest that the martian mantle has evolved with a Re/Os ratio within the range of chondrite meteorites. Combined with the HSE abundances of shergottites, the Re–Os isotope compositions and HSE abundances of Y 984028 (and other shergottites) may be generated from a martian mantle with abundances and proportions of these elements approaching values akin to the primitive upper mantle of Earth (Becker et al., 2006), which contains significantly greater concentrations of HSE than estimated for the lunar mantle (Day et al., 2007, 2010). The estimated chondritic-relative HSE abundances of the martian mantle, from Y 984028 and other shergottites, are in excess of those predicted by models of low-pressure core mantle differentiation, and may require accretion of meteoritic material (with broadly chondritic Re/Os) following core formation (e.g., Brandon et al., 2000; Walker, 2009), the timing of which is poorly resolved.

5. Summary

Y 984028 is a lherzolitic shergottite that contains Mg-rich minerals in poikilitic and non-poikilitic zones, as compared with more Fe-rich minerals such as those in LEW 88516. Constituent minerals are not in Fe–Mg equilibrium with the whole rock, demonstrating a cumulate origin for this meteorite. The textural characteristics and crystallization sequence observed in the present study are similar to those noted in several other lherzolitic shergottites. Oxygen isotopes confirm the martian origin of this sample, and slightly low $\Delta^{17}O$ may represent a magmatic signature. Y 984028 is likely paired with Y 000027, Y 000047, Y 000097, but is also similar to other lherzolitic shergottites (e.g., Y 793605, GRV 99027, and ALHA 77005). The unusual monomict breccia in Zone C of Y 984028, 51–3 indicates that this lherzolitic shergottite may have experienced some cataclastic fragmentation during ejection from Mars, but further study is required to confirm the origin of this breccia. Trace-element characteristics are similar to those in other lherzolitic shergottites, and are within error of those reported for ALHA 77005, LEW 88516, and Y 000097. Assimilation of meteoritic material does not account for the observed HSE abundances and Re–Os isotope characteristics of lherzolitic shergottites. The Re–Os isotope system provides a broadly chondritic initial $^{187}Os/^{188}Os$ value of 0.1281(2) (at 170 Ma) in Y 984028 that is similar to the osmium isotope composition of other lherzolitic shergottites and may reflect an average time-integrated martian mantle Re/Os value within the range of chondritic meteorites.

Acknowledgements

This work was completed as part of a consortium study organized by the National Institute for Polar Research to characterize Y 984028, to constrain its petrogenesis and relationship to other shergottites. We are grateful to R.D. Ash for technical assistance with LA-ICP-MS analyses, and to Allan Patchen for his help during EMP analyses. We appreciate constructive comments from J. Filiberto, an anonymous reviewer, and the associate editor, A. Yamaguchi, which helped to improve this manuscript. Funding was provided by NASA Cosmochemistry grants NNX08AG54G (LAT) and NNX07AM29G (RJW) for which we are very appreciative. In addition, partial funding was provided by the Planetary Geosciences Institute at UT.

Appendix. Supplementary material

Supplementary data associated with this article can be found in the online version, at doi:10.1016/j.polar.2010.04.009.

References

Anders, E., Grevesse, N., 1989. Abundances of the elements; meteoritic and solar. Geochimica et Cosmochimica Acta 53 (1), 197–214.

Anderson, D.J., Lindsley, D.H., Davidson, P.M., 1993. QUILF: a Pascal program to assess equilibria among Fe–Mg–Mn–Ti oxides, pyroxenes, olivine, and quartz. Computers and Geosciences 19 (9), 1333–1350.

Basu Sarbadhikari, A.M., Day, J.M.D., Liu, Y., Rumble, D., Taylor, L.A., 2009. Petrogenesis of olivine-phyric shergottite Larkman Nunatak 06319: implications for enriched components in Martian basalts. Geochimica Et Cosmochimca Acta 73 (7), 2190–2214.

Beck, A.W., McSween, Jr., H.Y., Mittlefehldt, D.W., Lee, C-T.A., 2009. "Fused bead analysis of diogenite meteorites". In: 40th Lunar and Planetary Science Conference, Abstract #1177.

Becker, H., Horan, M.F., Walker, R.J., Gao, S., Lorand, J.-P., Rudnick, R.L., 2006. Highly siderophile element composition of the Earth's primitive upper mantle: constraints from new data on peridotite massifs and xenoliths. Geochimica Et Cosmochimica Acta 70 (17), 4528–4550.

Birck, J.-L., Roy-Barman, M., Capmas, F., 1997. Re–Os isotopic measurements at the femtomole level in natural samples. Geostandard Newsletter 20, 19–27.

Blanchard, M.B., Cunningham, G.G., 1974. Artificial meteor ablation studies: olivine. Journal of Geophysical Research-Solid Earth 79 (26), 3973–3980.

Blinova, A., Herd, C.D.K., 2009. Experimental Study of polybaric REE partitioning between olivine, pyroxene and melt of the Y 980459 composition: insight into the petrogenesis of depleted shergottites. Geochimica Et Cosmochimica Acta 73, 3471–3492.

Bogard, D.D., Johnson, P., 1983. Martian gases in an Antarctic meteorite. Science 221 (4611), 651–654.

Borg, L., Nyquist, L.E., Weismann, H., Shih, C.-Y., Reese, Y., 2002. Constrains on the petrogenesis of Martian meteorites from the partially disturbed Rb–Sr and Sm–Nd isotopic systematics of LEW88516 and ALH77005. Geochimica Et Cosmochimica Acta 66, 2037–2053.

Borg, L.E., Draper, D.S., 2003. A petrogenetic model for the origin and compositional variation of the Martian basaltic meteorites. Meteoritics and Planetary Science 38 (12), 1711–1875.

Borg, L.E., Nyquist, L.E., Weismann, H., Shih, C.-Y., Reese, Y., 2003. The age of Dar Al Gani 476 and the differentiation history of the Martian meteorites inferred from their radiogenic isotopic systematics. Geochimica Et Cosmochimica Acta 67 (18), 3519–3536.

Brandon, A.D., Walker, R.J., Morgan, J.W., Goles, G.G., 2000. Re–Os isotopic evidence for early differentiation of the Martian mantle. Geochimica Et Cosmochimica Acta 64 (23), 4083–4095.

Brandon, A.D., Walker, R.J., Puchtel, I.S., Irving, A.J., 2008. "Re–Os Isotope Systematics of the Shergottite "Depleted" End-Member". 39th Lunar and Planetary Science Conference, Abstract #1404.

Brandstätter, F., Brack, A., Baglioni, P., Cockell, C.S., Demets, R., Edwards, H.G.M., Kurat, G., Osinski, G.R., Pilliniger, J.M., Roten, C.-A., Sancisi-Frey, S., 2008. Mineralogical alteration of artificial meteorites during atmospheric entry. The STONE-5 experiment. Planetary and Space Science 56 (7), 976–984.

Brown, R.W., 1977. A sample fusion technique for whole-rock analysis with the electron microprobe. Geochimica Et Cosmochimica Acta 41 (3), 435–438.

Calvin, C., Rutherford, M., 2008. The parental melt of lherzolitic shergottite ALH 77005: a study of rehomogenized melt inclusions. American Mineralogist 93, 1886–1898.

Cohen, A.S., Waters, F.G., 1996. Separation of osmium from geological materials by solvent extraction for analysis by thermal ionisation mass spectrometry. Analytica Chimica Acta 332 (2–3), 269–275.

Creaser, R.A., Papanastassiou, D.A., Wasserburg, G.J., 1991. Negative thermal ion mass spectrometry of osmium, rhenium and iridium. Geochimimica Et Cosmochimica Acta 55, 397–404.

Day, J.M.D., Taylor, L.A., Valley, J.W., Spicuzza, M.J., 2005. Assimilation of high $^{18}O/^{16}O$ crust by shergottite-nakhlite-chassigny (SNC) magmas on Mars. EOS Trans. AGU Fall Meeting Suppl. 86 (52) Abstract P51A-0902.

Day, J.M.D., Taylor, L.A., Floss, C., Patchen, A.D., Schnare, D.W., Pearson, D.G., 2006a. Comparative petrology, geochemistry and petrogenesis of evolved, low-Ti lunar mare basalt meteorites from the La Paz icefield, Antarctica. Geochimica Et Cosmochimica Acta 70, 1581–1600.

Day, J.M.D., Taylor, L.A., Floss, C., McSween Jr., H.Y., 2006b. Petrology and chemistry of MIL 03346 and its significance in understanding the petrogenesis of nakhlites on Mars. Meteoritics and Planetary Science 41 (4), 495–662.

Day, J.M.D., Pearson, D.G., Taylor, L.A., 2007. Highly siderophile element constraints on accretion and differentiation of the Earth–Moon system. Science 315, 217–219.

Day, J.M.D., Walker, R.J., James, O.B., Puchtel, I.S., 2010. Osmium isotope and highly siderophile element systematics of the lunar crust. Earth and Planetary Science Letters 289, 595–605.

Debaille, V., Brandon, A.D., Yin, Q.-Z., Jacobsen, B., 2007. Coupled $^{142}Nd-^{143}Nd$ evidence for the protracted magma ocean in Mars. Nature 450, 525–528.

Debaille, V., Yin, Q.-Z., Brandon, A.D., Jacobsen, B., 2008. Martian mantle mineralogy investigated by the $^{176}Lu-^{176}Hf$ and $^{147}Sm-^{143}Nd$ systematics of shergottites. Earth and Planetary Science Letters 269 (1–2), 186–199.

Elkins-Tanton, L.T., Parmentier, E.M., Hess, P.C., 2003. Magma ocean fractional crystallization and cumulate overturn in terrestrial planets: implications for Mars. Meteoritics & Planetary Science 38 (12), 1753–1771.

Filiberto, J., Jackson, C., Le, L., Treiman, A.H., 2009. Partitioning of Ni between olivine and an iron-rich basalt: experiments, partition models, and planetary implcations. American Mineralogist 94 (2–3), 256–261.

Ford, C.E., Russell, D.G., Craven, J.A., Fisk, M.R., 1983. Olivine-liquid equilibria: temperature, pressure and composition dependence of the crystal/liquid cation partition coefficients for Mg, Fe^{2+}, Ca and Mn. Journal of Petrology 24 (3), 256–266.

Franchi, I.A., Wright, I.P., Sexton, A.S., Pillinger, C.T., 1999. The oxygen isotope composition of Earth and Mars. Meteoritics and Planetary Science 34, 657–661.

Gale, N.H., Arden, J.W., Hutchinson, R., 1975. The chronology of the Nakhla achondritic meteorite. Earth and Planetary Science Letters 26 (2), 195–206.

Gillet, P., Barrat, J.A., Beck, P., Marty, B., Greenwood, R.C., Franchi, I.A., Bohn, M., Cotton, J., 2005. Petrology, geochemistry, and cosmic-ray exposure age of lherzolitic shergottite Northwest Africa 1950. Meteoritics & Planetary Science 40 (8), 1175–1184.

Goodrich, C.A., 2002. Olivine-phyric Martian basalts: a new type of shergottite. Meteoritics and Planetary Science 37, 31–34.

Harvey, R.P., Wadhwa, M., McSween Jr., H.Y., Crozaz, G., 1993. Petrography, mineral chemistry, and petrogenesis of Antarctic shergottite LEW-88516. Geochimica Et Cosmochimica Acta 57 (19), 4769–4783.

Herd, C.D.K., Borg, L.E., Jones, J.H., Papike, J.J., 2002. Oxygen fugacity and geochemical variations in the Martian basalts, implications for Martian basalt petrogenesis and the oxidation state of the upper mantle of Mars. Geochimica Et Cosmochimica Acta 66 (11), 2025–2036.

Horan, M.F., Walker, R.J., Morgan, J.W., Grossman, J.N., Rubin, A.E., 2003. Highly siderophile elements in chondrites. Chemical Geology 196 (1–4), 27–42.

Hu, S., Feng, L., Ling, Y.T., 2009. Petrography and mineral chemistry of Y984028 Lherzolitic shergottite. In: 32nd Symposium on Antarctic Meteorites.

Ikeda, Y., 1997. Petrology and mineralogy of Y-793605 Martian meteorite. Antarctic Meteorite Research 10, 13–40.

Ikeda, Y., 1998. Petrology and magmatic silicate inclusions in the ALH77005 lherzolitic shergottite. Meteoritics & Planetary Science 33, 803–812.

Ireland, T.J., Walker, R.J., Garcia, M.O., 2009. Highly siderophile element and ^{187}Os isotope systematics of Hawaiian picrites: implications for parental melt composition and source heterogeneity. Chemical Geology 260, 112–128.

Jones, J.H., 1989. "Isotopic relationships among the shergottites, the nakhlites and chassigny". In: Proceedings of the 19th Lunar and Planetary Science Conference, p. 465−474.

Lodders, K., 1998. A survey of shergottite, nakhlite and chassigny meteorites whole-rock compositions. Meteoritics and Planetary Science 33, 183−190.

McSween Jr., H.Y., 1994. What we have learned about Mars from SNC meteorites. Meteoritics 29 (6), 757−779.

McSween Jr., H.Y., Treiman, A.H., 1998. Martian meteorites. In: Ribbe, P.H. (Ed.), Planetary Materials (chapter 6).

McSween Jr., H.Y., 2002. The rocks of Mars, from far and near. Meteoritics and Planetary Science 37, 7−25.

McSween Jr., H.Y., 2003. Mars. In: Davis, A.M. (Ed.), Treatise on Geochemistry, pp. 601−622.

McSween Jr., H.Y., Taylor, G.J., Wyatt, M.B., 2009. Elemental composition of the Martian crust. Science 324 (5928), 736−739.

Meyer, C., 2009. The Mars meteorite compendium. http://www-curator.jsc.nasa.gov/antmet/mmc/.

Mikouchi, T., Miyamoto, M., 1997. Yamato-793605: a new lherzolitic shergottite from the Japanese Antarctic meteorite collection. Antarctic Meteorite Research 10, 41−60.

Mikouchi, T., Kurihara, T., 2008. Mineralogy and petrology of paired lherzolitic shergottites Yamato 000027, Yamato 000047, and Yamato 000097: another fragment from a Martian "lherzolitic" block. Polar Science 2 (3), 175−194.

Mikouchi, T., Satake, W., Kurihara, T., 2009. Y984028 lherzolitic shergottite: a new Antarctic find likely paired with Y000027/Y000047/Y000097. 32nd Symposium on Antarctic Meteorites.

Misawa, K., Yamada, K., Nakamura, N., Morikawa, N., Yamashita, K., Predo, W.R., 2006. Sm−Nd isotopic systematics of lherzolitic shergottite Yamato-793605. Antarctic Meteorite Research 19, 45−47.

Misawa, K., Park, J., Shih, C.-Y., Reese, Y., Bogard, D.D., Nyquist, L.E., 2008. Rb−Sr, Sm−Nd, and Ar−Ar isotopic systematics of lherzolitic shergottite Yamato 000097. Polar Science 2 (3), 163−174.

Misawa, K., Greenwood, R.C., Franchi, I.A., Kaiden, H., Kojima, H., 2009. New shergottites, Y980497 and Y984028, from the Yamato Mountains. 32nd Symposium of Antarctic Meteorites.

Morikawa, N., Misawa, K., Kondorosi, G., Premo, W.R., Tatsumoto, M., Nakamura, N., 2001. Rb−Sr isotopic systematics of lherzolitic shergottite Yamato-793605 lherzolite. Antarctic Meteorite Research 14, 47−60.

Nakamura, N., Komi, N., Kagami, H., 1982. Rb−Sr isotopic and REE abundances in the chassigny meteorite. Meteoritics 17, 257.

Nyquist, L.E., Bogard, D.D., Shih, C.-Y., Greshake, A., Stöffler, D., Eugster, O., 2001. Ages and geologic histories of Martian meteorites. Space Science Reviews 96 (1−4), 105−164.

Nyquist, L.E., Shih, C-Y., Reese, Y.D., 2006. Initial isotopic heterogeneities in Zagami: evidence of a complex Magmatic history. 69th Meeting of the Meteritical Society, Zurich, Switzerland.

Ostertag, R., Amthauer, D., Rager, H., McSween Jr., H.Y., 1984. Fe^{3+} in shocked olivine crystals of the ALHA 77005 meteorite. Earth and Planetary Science Letters 67 (2), 162−166.

Papike, J.J., Karner, J.M., Shearer, C.K., 2003. Determination of planetary basalt parentage: a simple technique using the electron microprobe. American Mineralogist 88, 469−472.

Papike, J.J., Karner, J.M., Shearer, C.K., Burger, P.V., 2009. Silicate mineralogy of Martian meteorites. Geochimica Et Cosmochimica Acta 73, 7443−7485.

Peucker-Ehrenbrink, B., Jahn, B.-M., 2001. Rhenium−osmium isotope systematics and platinum group element concentrations: loess and the upper continental crust. Geochem. Geophys. Geosyst 2 (10), 1061.

Puchtel, I.S., Walker, R.J., James, O.B., Kring, D.A., 2008a. Osmium isotope and highly siderophile element systematics of lunar impact melt breccias: implications for the late accretion history of the Moon and Earth. Geochimica Et Cosmochimica Acta 72 (12), 3022−3042.

Puchtel, I.S., Walker, R.J., Brandon, A.D., Irving, A.J., 2008b. Highly siderophile element abundances in SNC meteorites: an update. 39th Lunar and Planetary Science Conference, Abstract # 4015.

Roeder, P.L., Emslie, R.F., 1970. Olivine-liquid euilibrium. Contributions to Mineralogy and Petrology 29 (4), 275−289.

Rumble, D., Hoering, T.C., 1994. Analysis of oxygen and sulfur isotope ratios in oxide and sulfide minerals by spot heating with a carbon-dioxide laser in a flourine atmosphere. Accounts of Chemical Research 27 (8), 237−241.

Rumble, D., Irving, A.J., 2009. Dispersion of oxygen isotopic compositions among 42 Martian meteorites determined by laser flourination: evidence of (ancient) altered crust. 40th Lunar and Planetary Science Conference, Abstract# 2293

Sharp, Z.D., 1990. A laser-based microanalytical method for the in situ determination of oxygen isotope ratios of silicates and oxides. Geochimica Et Cosmochimica Acta 54 (5), 1353−1357.

Shearer, C.K., Burger, P.V., Papike, J.J., Borg, L.E., Irving, A.J., Herd, C., 2008. Petrogenetic linkages among Martian basalts. implications based on trace element chemistry of olivine. Meteoritics and Planetary Science 43, 1241−1258.

Shih, C.Y., L.E., Nyquist, Reese, Y., Misawa, K., 2009. Rb−Sr isotopic studies of Antarctic lherzolitic shergottite Yamato 984028. 32nd Symposium on Antarctic Meteorites.

Shirai, N., Ebihara, M., 2009. Chemical characteristics of lherzolitic shergottite Yamato 000097: magmatism on Mars inferred from the chemical composition of shergottites. Polar Sciences 3 (2), 117−133.

Stockstill, K.R., Bodnar, R.J., McSween Jr., H.Y., Benedix, G.K., 2001. Melt inclusions in Nakhla and ALHA 77005: indicators of parental magmas on Mars. Meteoritics & Planetary Science 36, A198.

Stöffler, D., Keil, K., Scott, E.R.D., 1991. Shock metamorphism of ordinary chondrites. Geochimica Et Cosmochimica Acta 55 (12), 3845−3867.

Symes, S.J.K., Borg, L.E., Shearer, C.K., Irving, A.J., 2008. The age of the Martian meteorite Northwest Africa 1195 and the differentiation history of the shergottites. Geochimica Et Cosmochimica Acta 72 (6), 1696−1710.

Thaisen, K.G., Taylor, L.A., 2009. Meteorite fusion crust variability. Meteoritics and Planetary Science 44 (6), 871−878.

Treiman, A.H., McKay, G.A., Bogard, D.D., Mittlefehldt, D.W., Wang, M.-S., Keller, L., Lipschutz, M.E., Lindsstrom, M.M., Garrison, D., 1994. Comparison of the LEW 88516 And ALHA 77005 Martian meteorites − similar but distinct. Meteoritics 29 (5), 581−592.

Trieman, A.H., Gleason, J.D., Bogard, D.D., 2000. The SNC meteorites are from Mars. Planetary and Space Science 48 (12−14), 1213−1230.

Treiman, A.H., 2003. Chemical compositions of Martian basalts (shergottites): some inferences on basalt formation, mantle metasomatism, and differentiation in Mars. Meteoritics and Planetary Sciences 38 (12), 1849−1864.

Wadhwa, M., 2001. Redox state of Mars' upper mantle and crust from Eu anomalies in shergottite pyroxenes. Science 291 (5508), 1527−1530.

Walker, R.J., Horan, M.F., Morgan, J.W., Becker, H., Grossman, J.N., Rubin, A.E., 2002. Comparative $^{187}Re-^{187}Os$ systematics of chondrites: implications regarding early solar system processes. Geochimica Et Cosmochimica Acta 66, 4187−4202.

Walker, R.J., 2009. Highly siderophile elements in the Earth, Moon and Mars: update and implications for planetary accretion and differentiation. Chemie Der Erde 69 (2), 101−125.

Warren, P.H., Kallemeyn, G.W., Kyte, F.T., 1999. Origin of planetary cores: evidence from highly siderophile elements in Martian meteorites. Geochimica Et Cosmochimica Acta 63 (13−14), 2105−2122.

Wooden, J., Shih, C-Y., Nyquist, L.E., Bansal, B., Wiesmann, H., McKay, G., 1982. "Rb−Sr and Sm−Nd isotopic constraints on the origin of EETA-79001: a second Antarctic shergottite". In: Proceeding of the 13th Lunar and Planetary Science Conference, p. 879−880.

Zipfel, J., Goodrich, C.A., 2001. REE in melt inclusions in Olivine of ALHA77005. Meteoritics & Planetary Science 36, A232.

NiPR
National Institute of Polar Research

INTERNATIONAL POLAR YEAR
2007-2008